Article

The Effect of Water on the Stability of Iron Oxide and Iron Carbide Nanoparticles in Hydrogen and Syngas Followed by in Situ X-ray Absorption Spectroscopy

Peter Thüne,*,[†] Prabashini Moodley,[‡] Freek Scheijen,[†] Hans Fredriksson,[†] Remco Lancee,[†] Jeremy Kropf,[§] Jeffrey Miller,[§] and J. W. (Hans) Niemantsverdriet[†]

[†]Schuit Institute of Catalysis, Eindhoven University of Technology, Eindhoven, The Netherlands
[‡]Iron Fischer–Tropsch Group, Sasol Technology, Sasolburg, South Africa
[§]Heterogeneous Catalysis Group, Argonne National Laboratory, Argonne, Illinois, United States

Ⓢ Supporting Information

ABSTRACT: The effect of water on iron-based nanoparticles under hydrogen and syngas was investigated by in situ X-ray absorption spectroscopy. The iron oxide (γ-Fe$_2$O$_3$) nanoparticles, dispersed as a monolayer on flat silica surfaces, were readily converted into metallic iron in dry hydrogen at 350 °C and into iron carbide in dry syngas (H$_2$/CO 2/1 vol/vol) at 325 °C. However, in the presence of water, the reduction did not proceed beyond magnetite (Fe$_3$O$_4$) up to 350 °C. Wustite (Fe(II)O or FeO$_{(1-x)}$) was formed at 450 °C in wet syngas and 550 °C in wet hydrogen. Once formed, the iron carbide nanoparticles proved remarkably stable against oxidation in wet syngas at 350 °C. However, we observed the formation of a surface iron(II) oxide phase that increases with increasing H$_2$O/CO ratio. This implies that the active surface of iron-based Fischer–Tropsch catalysts is covered by considerable amounts of adsorbed oxygen during the Fischer–Tropsch reaction. Reducing the temperature by only 20 K results in complete and irreversible oxidation to magnetite. We propose that the surface iron(II) oxide plays an important role during Fischer–Tropsch synthesis by regulating the relative rates of CO hydrogenation versus water gas shift and by stabilizing the iron carbide catalyst against irreversible deactivation by oxidation to magnetite.
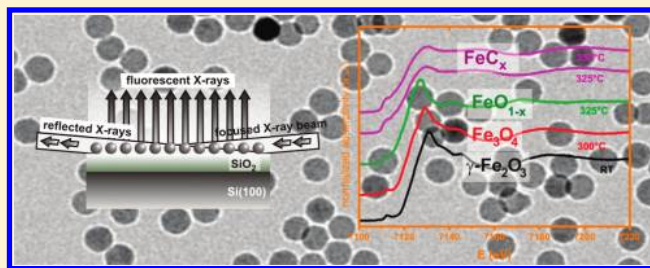
■ INTRODUCTION

Iron-based Fischer–Tropsch catalysts have received much renewed interest in recent years due to their unique ability to transform syngas from carbon-rich sources (biomass, coal) to a variety of useful products, including diesel fuel, short chain alkenes, and oxygenates.[1−5]

While the actual FT reaction (2H$_2$ + CO ↔ "−CH2−" + H$_2$O) is believed to take place at the surfaces of iron carbides, iron oxides (magnetite) are held responsible for the production of additional hydrogen by catalyzing the water gas shift (WGS) reaction (H$_2$O + CO ↔ CO$_2$ + H$_2$).

Recent literature has focused on in-depth characterization of the active iron catalyst[4,6−10] and on kinetic and theoretical modeling.[11−15] However, many fundamental issues regarding iron-based FT catalysis, such as mechanism and structure reactivity relations, remain unsettled. This uncertainty stems, in part, from the dynamic and complex nature of the iron active phase in the reaction medium.[16] During the FT reaction, typically, a multitude of iron-containing phases coexist, including iron oxides, metallic iron, and iron carbides. In addition, the composition and reactivity of the catalyst nanoparticles will respond to the local concentrations of the reactive gases (H$_2$, CO, CO$_2$, and H$_2$O), which, in turn, are a function of the overall conversion and the local activity.

Addition of promoters, such as alkali metals, copper, and silica, further add to the structural complexity of iron-based Fischer–Tropsch catalysts. X-ray microscopy performed on iron-based FT catalysts under reaction conditions has demonstrated that these catalysts are highly heterogeneous regarding their constituent iron phases and that these phases coexist within a few 10 nm from each other.[17]

In a typical model catalyst approach, we have set out to simplify this catalyst by applying monodisperse maghemite (γ-Fe$_2$O$_3$) precursors onto flat silicon oxide membranes.[18] Such model catalysts are ideally suited for an in-depth characterization by X-ray photoelectron spectroscopy (XPS), transmission electron spectroscopy (TEM), and X-ray absorption spectroscopy (XAS). All supported iron oxide nanoparticles are equally accessible to a well-defined reaction medium as changes in the gas composition induced by the catalytic reaction are negligible. Therefore, the iron oxide nanoparticles dispersed on planar supports will show a more homogeneous phase behavior in a reactive environment than in porous 3-dimensional agglomerates typical for industrial catalysts.

Here, we will concentrate on the chemical transformations of the supported iron oxide nanoparticles in wet and dry H_2 and H_2/CO (2/1 vol/vol) mixtures, which are followed by in situ X-ray absorption spectroscopy. We will demonstrate that the initial maghemite nanoparticles convert into magnetite (Fe_3O_4) at 250−300 °C. These magnetite particles convert to metallic iron at 350 °C and to iron carbide at 325 °C in dry hydrogen and syngas, respectively. In both cases, the reaction proceeds via a wustite ($FeO_{(1-x)}$) phase. In wet syngas and hydrogen, the magnetite nanoparticles are much more stable and are only converted to wustite at high temperatures. During the Fischer−Tropsch reaction, water is formed as the main byproduct. Especially for high conversions, this raises the question about the stability of the active iron carbide phase against oxidation. By carefully controlling the temperature and the water/carbon monoxide ratio, we were able to follow the oxidation of iron carbide to magnetite in detail. At the onset of this oxidation, we detect and quantify an intermediate iron oxide phase, which we assign to be surface Fe(II)O. To our knowledge, this is the first time that iron(II)oxide was detected on the iron carbide surface under Fischer−Tropsch conditions.

■ EXPERIMENTAL SECTION

The flat FeO_x/SiO_2 model catalysts were prepared by spin-coating a colloidal solution of maghemite nanoparticles (18 nm average diameter) in toluene onto flat silica surfaces[19] (precalcined silicon wafers or silica TEM supports). The details of catalyst preparation and the custom-made silica TEM supports are described elsewhere.[18,20]

TEM images were recorded in an FEI Technai 20 (Sphera) transmission electron microscope operating at 200 kV. In situ XAS measurements at the Fe K edge were performed in grazing incidence fluorescence mode on the 10ID beamline at Argonne National Laboratory's Advanced Photon Source. The model catalyst wafers were placed horizontally in a reactor and carefully aligned in the X-ray beam to optimize the fluorescence signal and to avoid X-ray diffraction signals stemming from the silicon support in the region of interest. Soller slits and a Mn filter were used to suppress the elastic and Compton scattering and to improve the Fe fluorescence signal-to-background ratio. The grazing incidence reactor was based on a design by Lee et al.[21] The sample sits on a ceramic heater plate mounted to a cooled aluminum block via very short ceramic spacers, minimizing the effects of thermal expansion as the sample temperature is changed. A second ceramic heater plate is above the sample, helping to ensure a uniform temperature in a 1.5 cm × 1.5 cm area on the lower plate. A rhodium-coated mirror serves the dual purposes of harmonics rejection and focusing the beam to about a 25 μm height (with a divergence of about 0.5 mrad), so as to have the greatest number of photons incident on the sample. The glancing angle was chosen as a compromise between enhancing the Fe fluorescence signal and having a slowly varying background as a function of energy that accommodates a simpler analysis.

The reaction gases H_2, CO, and He were at least 99.99% pure and used without further purification. However, volatile metal carbonyls (i.e., $Fe(CO)_5$) in the CO were decomposed into metals over quartz wool at 350 °C in a separate heating zone prior to exposure to the catalyst. The total gas flow was maintained at 300 mL/min at atmospheric pressure. Optionally, water was added to the combined gas flow by passing through a stainless steel saturator at room temperature, resulting in a water content of 2.6%. By diluting the syngas stream (H_2/CO,

2/1 vol/vol) with helium while maintaining the total gas flow through the saturator constant, we could vary the CO/H_2O ratio in the syngas feed between 0.07 and 1.15, thereby emulating a conversion level of the FT reaction between 7% and 53%. The water content of the reaction gas was measured at all times at the exhaust of the reactor using a Mitchel MDM300 advanced dewpoint meter. In the following discussion, a water content of about 2.6 vol % is referred to as a "wet" gas stream, and a "dry" gas stream corresponds to a water content below 300 ppm.

■ RESULTS AND DISCUSSION

Upon heating the flat FeO_x/SiO_2 model catalysts in the presence of the gases (H_2, CO, He, H_2O) in the in situ XAS reactor, we could distinguish five stable iron phases, which we assign to maghemite (γ-Fe_2O_3), magnetite (Fe_3O_4), wustite (FeO_{1-x}), metallic iron (α-Fe), and iron carbide (FeC_x). Figure
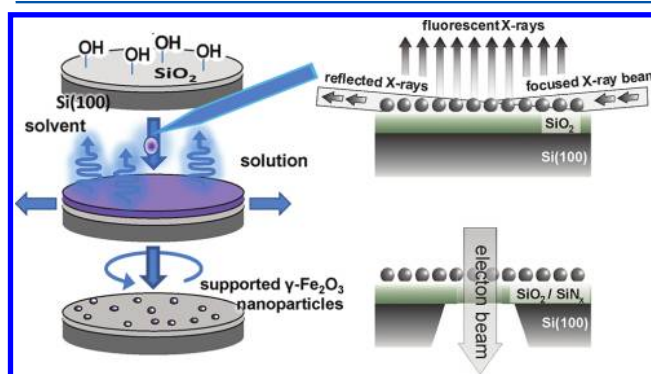

Figure 1. Left: preparation of a flat FeO_x/SiO_2 model catalyst by spin-coat impregnation starting from a silicon wafer covered by a 20 nm thick layer of silicon oxide. Top right: schematic representation of an in situ XAS measurement performed in grazing incidence fluorescence mode. Bottom right: schematic cross section through FeO_x nanoparticles supported on a silica TEM grid.

2 shows the in situ Fe K-edge spectra of these iron phases together with the composition and temperature under which the spectra were recorded. Also shown in Figure 1 are XAS reference spectra taken from oxide powders and metal foils, demonstrating good agreement with the spectra taken from the supported nanoparticles, thus correlating each in situ spectra of the model catalyst to the respective iron phases. (For a more detailed comparison, we refer to the Supporting Information.)

However, the exact nature of the iron carbide phase proves difficult to discern from XAS. Comparing our in situ XAS spectra in syngas with Fe_3C and Fe_5C_2 reference spectra kindly made available by Prof. Bert Weckhuysen and Dr. Emiel de Smit (Figure S4, Supporting Information) reveals a good qualitative agreement of our carburized model catalyst with both the external references; however, we cannot assign our iron carbide based on this comparison. On the other hand, De Smit et al. report in ref 22 that an α-Fe_2O_3 catalyst treated under similar condition as ours (20% CO in H_2 at 350 °C) predominantly consists of crystalline χ-Fe_5C_2. At this moment, we tentatively assign our FeC_x reference to be χ-Fe_5C_2 and emphasize that the in situ XAS spectra are very stable in time and reproducible.

The stability of the supported model catalyst against sintering was confirmed with TEM. Figure 3 shows the distribution of iron oxide nanoparticles on the flat silica membranes after
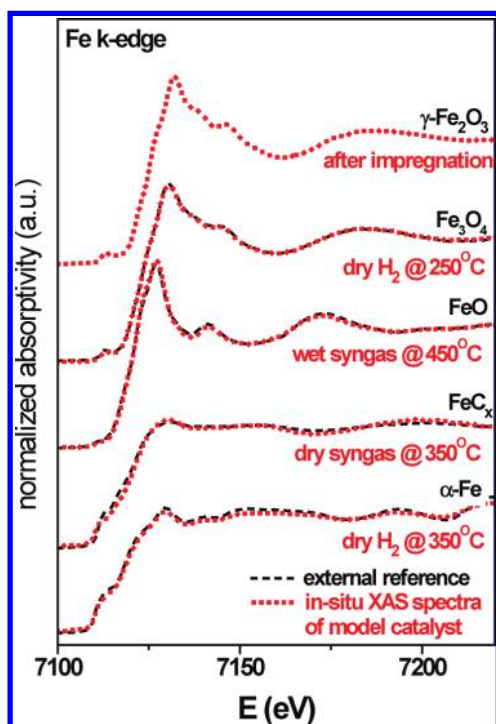
Figure 2. Normalized Fe K-edge spectra of the 18 nm FeO_x/SiO_2 model catalyst after transformation into different reference states under specified reaction conditions in comparison with external references. The in situ spectra of the model catalysts depicted here are used as internal references throughout the paper. For details, see text and the Supporting Information.

Figure 3. TEM images of the 18 nm FeO_x/SiO_2 model catalyst as deposited and after reduction in dry hydrogen at 400 °C. The insets show the corresponding electron diffractograms.

impregnation and after reduction in dry hydrogen at 400 °C. The inset shows the corresponding electron diffractograms. After reduction, the diffraction pattern corresponding to maghemite/magnetite has completely disappeared. The strongest remaining diffraction ring at about 0.2 nm corresponds to the 110 lattice fringes of metallic α-iron. The solid, spherical magnetite particles are transformed into core–shell particles with a metallic core and a shell of amorphous oxide, which has formed during sample transfer through a glovebox ambient. Even though sample transfer has altered the morphology of the hydrogen reduced particles, we are able to establish that most iron particles, which are supported on a flat silica membrane, do not coalesce during reduction at 400 °C.

The conversion of the supported γ-Fe_2O_3 into iron carbide or metallic iron proceeds in a stepwise fashion via magnetite and wustite.[23,24] Figure 4 shows the in situ XANES spectra of the FeO_x/SiO_2 model catalysts during reduction in dry hydrogen (left) and dry syngas (CO/H_2 2/1 vol/vol; right) as a function of reaction temperature . In both cases, the maghemite precursor is transformed into magnetite between 250 and 300 °C. At 350 °C in hydrogen, the magnetite nanoparticles are converted first into wustite and then into metal. The transformation from magnetite into iron carbide occurs around 325 °C in dry syngas. Again, wustite appears as a transient phase. Metallic iron cannot be observed during the conversion of wustite into iron carbide.

When the FeO_x/SiO_2 model catalyst is treated with wet hydrogen or syngas, the maghemite nanoparticles are much more stable against further reduction. At 350 °C, they have changed only to magnetite, and even as temperatures reach 550 °C, they are not converted beyond wustite (Figure 5). Note
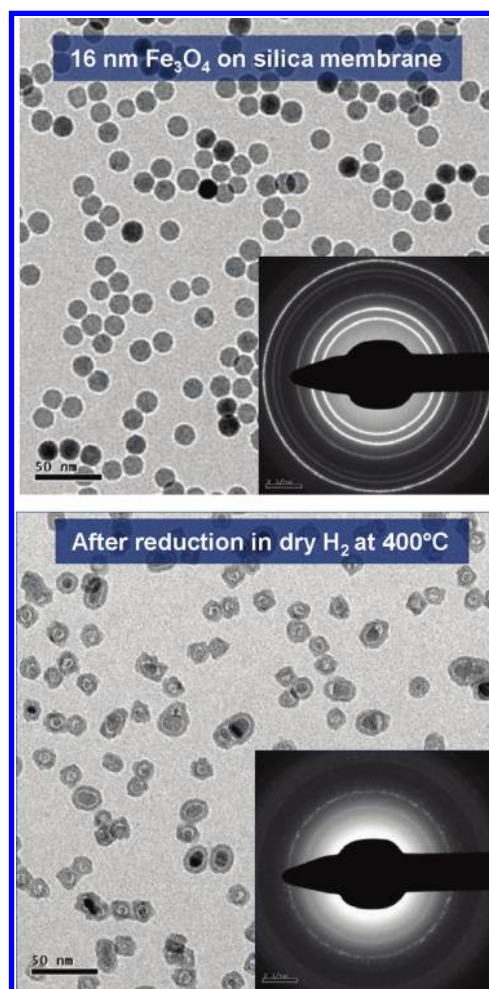
that the reduction to wustite occurs in wet syngas at a considerably lower temperature than in wet hydrogen, indicating that syngas is a more powerful reducing agent than hydrogen. Altogether, these results indicate that the transformation of magnetite into iron carbide requires very dry syngas in the absence of a reduction promoter like copper. Oxidation of the active iron carbide phase to inactive magnetite is, therefore, an obvious deactivation pathway for the iron-based FT catalyst.

To look deeper into the reoxidation of iron carbide by water in the syngas feed, we transformed the iron oxide nanoparticles of our model catalyst into iron carbide at 350 °C in dry syngas and then switched to wet syngas at this temperature. The carbide remains stable even upon cooling to 250 °C. At 200 °C, we observe a slow oxidation to magnetite (not shown for brevity).

After saturation at room temperature, the syngas stream (CO/H_2 2/1 vol/vol) contains 2.6 vol % water, corresponding to a H_2O/CO ratio of 0.07. However, by diluting the syngas stream with helium (while maintaining the total gas flow through the saturator constant), we achieve H_2O/CO ratios up to 1.15.

With this procedure, we emulate conditions corresponding to the Fischer–Tropsch reaction ($2H_2 + CO \rightarrow$ "CH_2" $+ H_2O$), reaching up to 53% conversion.
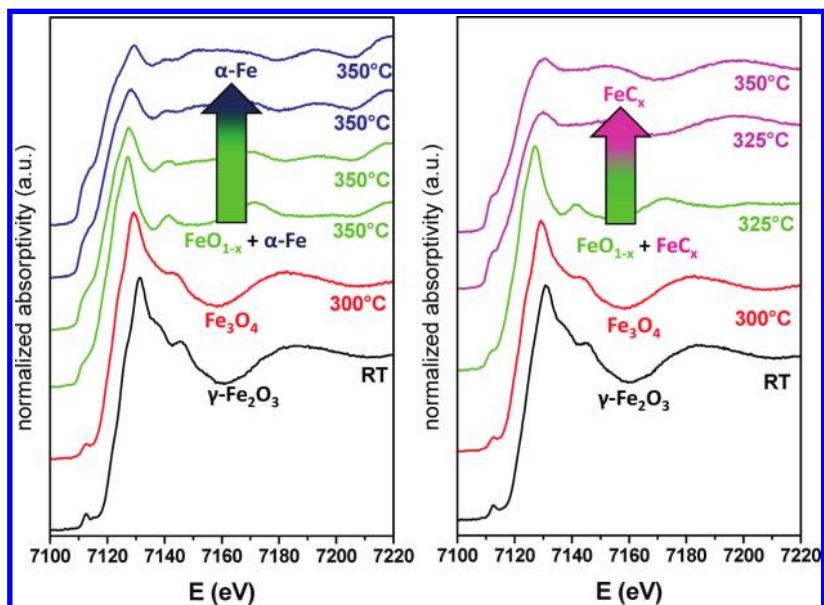
Figure 4. Normalized Fe K-edge spectra of the model catalyst during in situ treatment with dry hydrogen (left) and dry syngas (right).
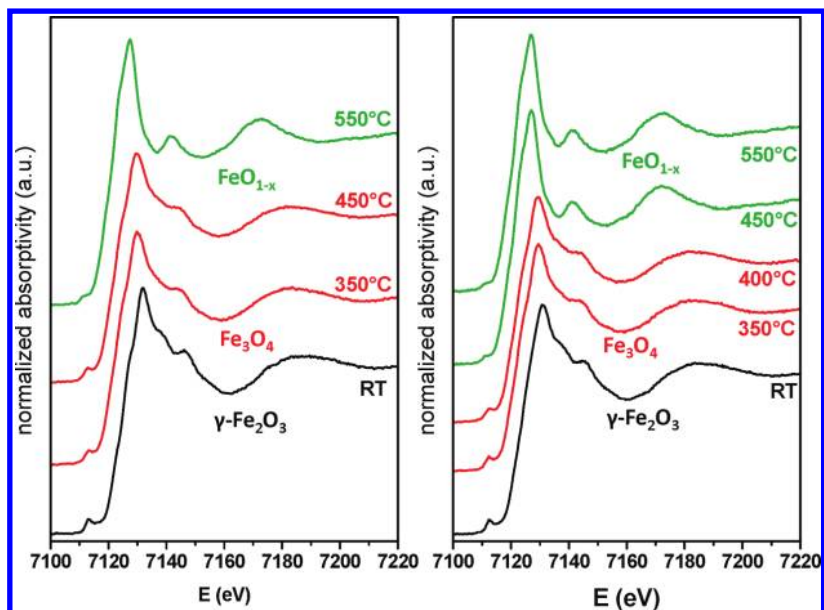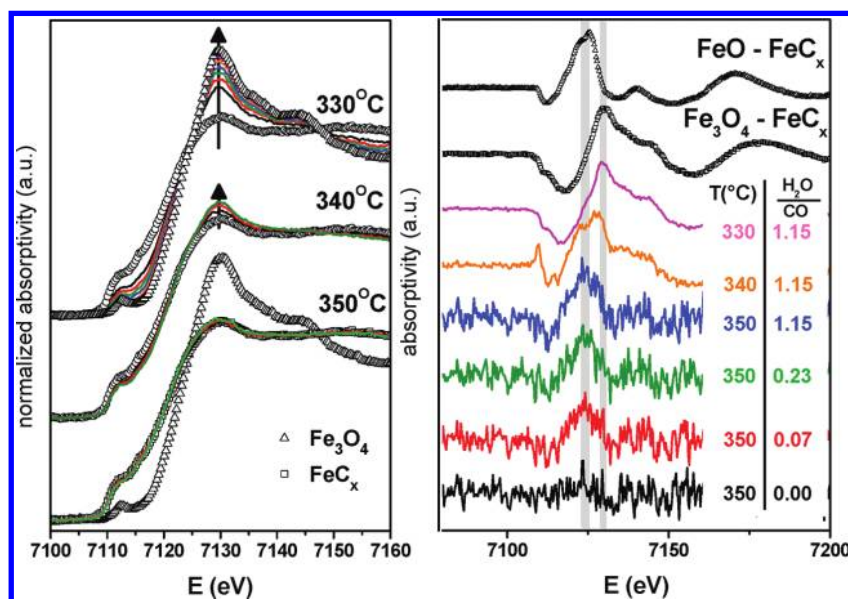

Figure 5. Normalized Fe K-edge spectra of the model catalyst during in situ treatment with wet hydrogen (left) and wet syngas (right).

The XANES spectra of this experiment are shown in Figure 6, left panel. Under these conditions, we observe only minute changes in the Fe K absorption edge, indicating a stable iron carbide phase. However, after cooling to 340 °C, we observe the onset of a gradual transformation of the carbide phase toward magnetite. This transformation completes within minutes after cooling to 330 °C. The subtle changes induced by the addition of water to the flowing syngas mixture at 350 °C become more clearly visible after subtracting the iron carbide reference spectrum from the in situ XANES spectra. The resulting difference spectra are shown on the right panel of Figure 6 together with two references (Fe(II)O and Fe_3O_4), both also after subtraction of the iron carbide reference. The bottom spectra taken at 350 °C show the evolution of a small, but significant, maximum at about 7124.5 eV that corresponds to the maximum of the Fe(II)O-FeC_x reference and is significantly different from the maximum of the Fe_3O_4-FeC_x

reference at 7130 eV. After cooling to 340 and 330 °C, the difference spectra start to resemble the Fe_3O_4-FeC_x reference.

Linear combination fitting using the magnetite, carbide, and wustite references confirms that the iron(II) oxide phase is initially the only oxide phase present and that the iron carbide is eventually converted completely to magnetite (Figure 7). At the onset of the magnetite formation at 340 °C, the iron(II) oxide phase is still present. The maximum contribution of the iron(II) oxide just before the magnetite becomes visible was determined to be 4% ± 1%, corresponding to a 0.2 nm thick surface layer, assuming spherical iron carbide particles. We believe that this is the first spectroscopic sighting of such surface iron(II) oxide on iron carbide under Fischer−Tropsch conditions. We could only detect this species because we used a well-defined model catalyst that features a single layer of iron oxide nanoparticles on a planar silica surface. This approach ensures that reaction conditions for all iron nanoparticles are

Figure 6. Left: normalized Fe K-edge spectra of iron carbide nanoparticles in wet syngas at 350, 340, and 330 °C. The solid traces are in situ XANES spectra, and the triangles and circles are the magnetite and carbide references, respectively. Right: the solid traces depict selected in situ XANES spectra after subtraction of the FeC_x reference spectra. The vertical lines mark the position of the maxima of the references at 7124.5 (Fe(II)O-FeC_x) and at 7130.0 eV (Fe_3O_4-FeC_x). Temperature and H_2O/CO ratio are indicated in the inset.
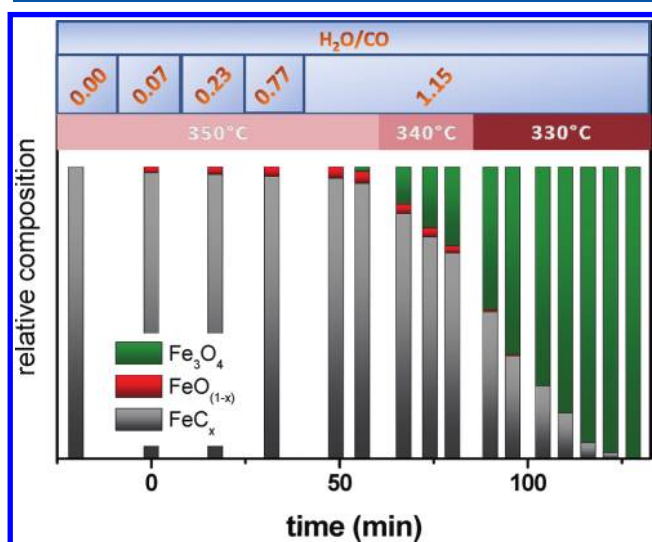
Figure 7. Evolution of the relative contributions of FeC_x, Fe_3O_4, and Fe(II)O in the model catalyst after switching from dry to wet syngas as derived from a linear combination fit of the XANES spectra shown in Figure 5. Temperature and H_2O/CO ratio are indicated above the bar graph.

the same and especially that the partial pressures of all relevant reaction gases are identical for all iron-based nanoparticles. On the other hand, the minute amount of active phase thus far prohibits the determination of catalytic activity.

Water is generally believed to promote oxidation of the active iron carbide and thus have an inhibiting effect on the FT rate while increasing the selectivity to CO_2 via the water gas shift (WGS) reaction.[25] However, on the basis of a review of kinetic models for iron-based FTS, Botes[3] suggests that water and CO_2 may have no direct kinetic effect on the FT activity at all but rather change the relative concentrations of CO and H_2 through an increased WGS activity. Pendyala et al. demonstrated that the effect of water cofeeding on an iron-based FT

catalyst (promoted with silica, potassium, and copper) is very sensitive to the reaction temperature.[26] At high temperatures (270 °C), the cofeeding of 10% water at a CO conversion level of about 50% resulted in an increased WGS activity, leaving the FT activity almost constant. However, at 230 °C, the total CO conversion was depressed drastically and irreversibly. This deactivation was linked to the oxidation of the iron carbide to magnetite.

Our results indicate that, in the presence of increasing amounts of water, the steady-state surface of the active iron carbide nanocrystals is converted to an oxygen-rich Fe(II) phase or—as an alternative description—the carbide surface becomes filled with chemisorbed oxygen. The removal of this adsorbed oxygen by hydrogen or carbon monoxide would regenerate the active surface for FT reaction. If we suppose that the surface iron oxide is active for the WGS reaction similarly to magnetite,[27] this surface would cause a depletion of the local water concentration, thereby creating a feedback loop controlling the FT and WGS reactivity as well as the stability of the iron carbide phase. When this balance is disturbed by decreasing the temperature or possibly increasing the water partial pressure, the oxidation proceeds beyond the surface iron(II) oxide and the carbide is quantitatively converted to magnetite. We have observed earlier that the reconversion of magnetite nanoparticles back to carbide is very difficult in the presence of even small amounts of water. Therefore, the oxidation of carbide to magnetite may, in practice, become an irreversible (partial) deactivation of the catalyst as the residual FT activity produces enough water to prohibit reactivation of magnetite.

Commercial FT catalysts operate at 330 °C (HTFTS) or even 230 °C (LTFTS) and routinely reach conversions exceeding 50% without (immediate) deactivation by oxidation to magnetite, as was observed with our model catalysts.[28] This apparent discrepancy can be explained bearing in mind that, in this model study, the amount of iron particles was too low to have any impact on the composition of the gas feed. Therefore,

we have excluded the effect of the water gas shift equilibrium ($CO + H_2O = CO_2 + H_2$) on the composition of the FT reaction mixture.

At 350 °C, WGS is very fast and strongly favors CO_2 and H_2. WGS leads to a drastic reduction of the water content in the FT reaction mixture. A decrease in water content leads to an increase in stability against reoxidation. In our model study, we were able to cool down FeC_x nanoparticles to below 250 °C in syngas containing 2.5% water ($H_2O/CO = 0.07$) without apparent oxidation.

CONCLUSION

Supporting catalytically active nanoparticles on flat silica surfaces offers a facile way to study the morphological and chemical changes of these particles under reactive conditions by (ex situ) TEM and (in situ) XAS. Because of the homogeneous nature of these model catalysts—with respect to particle size and distribution as well as with respect to their exposure to the reactive gases—their phase behavior under reaction conditions also becomes homogeneous.

We have demonstrated that iron oxide nanoparticles supported on flat silica are readily converted into metal, carbide, magnetite, and wustite nanoparticles within an in situ XAS flow reactor setup.

While complete conversion into metal and carbide is observed at 350 °C in dry hydrogen and syngas (H_2/CO 2/1 vol/vol), respectively, the addition of 2.6% water prevents the conversion to metal or carbide. Instead, at 350 °C, a stable magnetite phase is formed that is only converted into wustite (Fe(II)oxide) at 450 °C in wet syngas and at 550 °C in wet hydrogen.

Once formed, iron carbide nanoparticles are remarkably stable in wet syngas at 350 °C even when increasing the H_2O/CO ratio to a value corresponding to 53% FT conversion. Instead of reoxidation toward magnetite, we observe the formation of a surface iron(II) oxide layer that increases up to a full monolayer coverage with increasing H_2O/CO ratio. Though we cannot correlate the surface characterization of the flat FeO_x/SiO_2 model catalyst to Fischer−Tropsch reactivity at this moment, our results imply that the removal of adsorbed oxygen from the active iron carbide surface becomes increasingly difficult in the presence of water and may become a rate-limiting factor for the hydrogenation of CO over iron-based FT catalysts.

We propose that the formation of the surface Fe(II)O layer may play an important role in regulating the relative rates of FT and WGS reactions, thereby controlling the local concentration of water at the active surface and thus stabilizing the iron carbide against further oxidation. The stability of the surface-oxidized iron carbide particles responds very sensitively to temperature. Decreasing the temperature by only 20 K causes the iron carbide particles to convert quantitatively into FT inactive magnetite. This oxidation is effectively irreversible as long as the reaction medium at the magnetite surface contains at least some water.

ASSOCIATED CONTENT

ⓈSupporting Information

The Supporting Information contains the Fe K absorption edges and the imaginary part of the k^2-weighted Fourier transform of the $FeO_x/SiO_2/Si(100)$ model catalysts measured in situ in grazing incidence fluorescence mode under selected reaction conditions. These spectra are compared to transmission XAS spectra of relevant reference compounds measured in transmission mode. Transients of the carburization and of the subsequent reoxidation of the $FeO_x/SiO_2/Si(100)$ model catalyst are shown together with the results of their respective linear combination fittings, which reveal the presence of iron(II) oxide in both transients. This material is available free of charge via the Internet at http://pubs.acs.org.

AUTHOR INFORMATION

Notes

The authors declare no competing financial interest.

ACKNOWLEDGMENTS

REFERENCES

(1) Demirbas, A. *Prog. Energy Combust. Sci.* **2007**, *33*, 1−18.

(2) Lu, Y. J.; Lee, T. *J. Nat. Gas Chem.* **2007**, *16*, 329−341.

(3) Botes, F. G. *Catal. Rev.* **2008**, *50*, 471−491.

(4) de Smit, E.; Weckhuysen, B. M. *Chem. Soc. Rev.* **2008**, *37*, 2758−2781.

(5) van Steen, E.; Claeys, M. *Chem. Eng. Technol.* **2008**, *31*, 655−666.

(6) de Smit, E.; Beale, A. M.; Nikitenko, S.; Weckhuysen, B. M. *J. Catal.* **2009**, *262*, 244−256.

(7) Janbroers, S.; Louwen, J. N.; Zandbergen, H. W.; Kooyman, P. J. *J. Catal.* **2009**, *268*, 235−242.

(8) de Groot, F. M. F.; de Smit, E.; van Schooneveld, M. M.; Aramburo, L. R.; Weckhuysen, B. M. *ChemPhysChem* **2010**, *11*, 951−962.

(9) de Smit, E.; de Groot, F. M. F.; Blume, R.; Havecker, M.; Knop-Gericke, A.; Weckhuysen, B. M. *Phys. Chem. Chem. Phys.* **2010**, *12*, 667−680.

(10) Ribeiro, M. C.; Jacobs, G.; Davis, B. H.; Cronauer, D. C.; Kropf, A. J.; Marshall, C. L. *J. Phys. Chem. C* **2010**, *114*, 7895−7903.

(11) Huo, C. F.; Li, Y. W.; Wang, J. G.; Jiao, H. J. *J. Am. Chem. Soc.* **2009**, *131*, 14713−14721.

(12) Gracia, J. M.; Prinsloo, F. F.; Niemantsverdriet, J. W. *Catal. Lett.* **2009**, *133*, 257−261.

(13) Gnanamani, M. K.; Keogh, R. A.; Shafer, W. D.; Shi, B. C.; Davis, B. H. *Appl. Catal., A* **2010**, *385*, 46−51.

(14) Govender, N. S.; de Croon, M. H. J. M.; Schouten, J. C. *Appl. Catal., A* **2010**, *373*, 81−89.

(15) Petersen, M. A.; van den Berg, J. A.; van Rensburg, W. J. *J. Phys. Chem. C* **2010**, *114*, 7863−7879.

(16) Li, S.; Ding, W.; Meitzner, G. D.; Iglesia, E. *J. Phys. Chem. B* **2001**, *106*, 85−91.

(17) de Smit, E.; Swart, I.; Creemer, J. F.; Hoveling, G. H.; Gilles, M. K.; Tyliszczak, T.; Kooyman, P. J.; Zandbergen, H. W.; Morin, C.; Weckhuysen, B. M.; et al. *Nature* **2008**, *456*, 222−U39.

(18) Moodley, P.; Scheijen, F. J. E.; Niemantsverdriet, J. W.; Thüne, P. C. *Catal. Today* **2010**, *154*, 142−148.

(19) Thüne, P. C.; Weststrate, C. J.; Moodley, P.; Saib, A. M.; van de Loosdrecht, J.; Miller, J. T.; Niemantsverdriet, J. W. *Catal. Sci. Technol.* **2011**, *1*, 689−697.

(20) Moodley, P.; Loos, J.; Niemantsverdriet, J. W.; Thüne, P. C. *Carbon* **2009**, *47*, 2002−2013.

(21) Lee, S.; Lee, B.; Seifert, S.; Vajda, S.; Winans, R. E. *Nucl. Instrum. Methods Phys. Res., Sect. A* **2011**, *649*, 200−203.

(22) de Smit, E.; Cinquini, F.; Beale, A. M.; Safonova, O. V.; van Beek, W.; Sautet, P.; Weckhuysen, B. M. *J. Am. Chem. Soc.* **2010**, *132*, 14928−14941.

(23) Wimmers, O. J.; Arnoldy, P.; Moulijn, J. A. *J. Phys. Chem.* **1986**, *90*, 1331−1337.

(24) Zielinski, J.; Zglinicka, I.; Znak, L.; Kaszkur, Z. *Appl. Catal., A* **2010**, *381*, 191−196.

(25) Dry, M. E.; Shingles, T.; Boshoff, L. J. *J. Catal.* **1972**, *25*, 99−104.

(26) Pendyala, V. R. R.; Jacobs, G.; Mohandas, J. C.; Luo, M.; Hussein, H. H.; Ji, Y.; Ribeiro, M. C.; Davis, B. H. *Catal. Lett.* **2010**, *140*, 98−105.

(27) Ratnasamy, C.; Wagner, J. P. *Catal. Rev.* **2009**, *51*, 325−440.

(28) Dry, M. E. *J. Chem. Technol. Biotechnol.* **2001**, *77*, 43−50.

7373

dx.doi.org/10.1021/jp210754k | *J. Phys. Chem. C* 2012, 116, 7367−7373